SMAR 2017 – Fourth Conference on Smart Monitoring,
Assessment and Rehabilitation of Civil Structures

SMAR 2017

Elastic-wave-based Imaging System for Detecting Voids in Concrete Structures

Jian-Hua Tong [1]

[1] Hungkuang University, Taichung, Taiwan

ABSTRACT: In this paper, a synthetic aperture focusing technique imaging system was proposed to reveal the voids in concrete structures. It combines the advantage of point-source/point-receiver scheme and synthetic aperture focusing technique to construct images like those scanned with a phase array system so it can detect defects deeper than conventional ultrasonic systems can do with high-energy elastic wave. Design concept of each component in this system, including an impact source generator, a transducer, a signal capturing unit and operation software, is clearly described. For usability evaluation, a concrete slab with an artificial defect was cast for experiment. A 2D plane-stress finite difference simulation on corresponding numerical module was carried out for comparison. The experimental result shows good agreement with the numerical result not only on the B-scan diagram but also on the resultant image. It exhibits the potential of the proposed imaging system in inspecting defects of in-situ concrete structures by image.

1. INTRODUCTION

In present NDT methods for civil engineering, elastic-wave-based methods have been successfully applied to inspect the integrity of concrete structures. The key to success is point-source/point-receiver scheme. It uses mechanical impact to generate high-energy elastic wave to overcome the limitation of functional depth caused by the nature of conventional ultrasonic probing which is low output power. Furthermore, the center frequency of generated elastic wave could be alternated by just changing corresponding size of steel ball to meet the required inspection resolution.

By adopting point-source/point-receiver scheme, Wu et al. proposed a method to measure elastic constants of concrete material nondestructively. In addition, they also proposed a method to measure the depth of a surface-breaking crack in concrete by detecting the longitudinal wave diffracted from crack tip. Later in 2001, Liu et al. proposed a method to reveal the depth of a surface-breaking crack in reinforced concrete by means of imaging. In impact-echo method, it transforms a time-domain signal into a frequency-domain signal and analyzes the response to detect voids inside concrete structures. By combing the advantage of the point-source/point-receiver scheme and SAFT (Synthetic Aperture Focusing Technique) process, Tong et al. proposed methods to imaging defects by extracting information from multiple received signals. The result shows the potential of these methods could be a practical and effective NDT tool to inspect defects inside concrete structures. In this paper, a portable defect imaging system basing on point-source/point-receiver scheme and SAFT process was proposed. Each component, including an impact source generator, a transducer, a signal capturing unit and operation

software, was carefully designed and calibrated to meet the requirement of on-site applications. A defective concrete slab was cast for the usability evaluation of this proposed system.

2. PRINCIPLE OF IMAGING METHOD

With conventional SAFT-imaging method, the resultant ultrasonography is as good as that obtained with a linear array system but no need to use complex apparatus. In this method, the measurement is performed just with one ultrasonic probe so the apparatus is much simpler than a linear array system. To match present NDT diagnosis scheme in civil engineering and also increase functioning depth, a conventional ultrasonic probe is replaced by a point-source/point-receiver set in the imaging system proposed in this paper. The measurement is completed with a point-source/point-receiver set separated a certain distance. As shown in Figure 1, a series of impact-and-receive operations is performed on the surface of a specimen. Let S_i and R_i represents the location of a set of source and receiver for the i-th measurement. Furthermore let $T_i(t)$ be the magnitude of the response signal recorded at R_i for this measurement. An image intensity $I(m,n)$ can be assigned to each grid based on the following calculation:

$$I(m,n) = \frac{1}{N}\sum_{i=1}^{N} T_i(t_i) \tag{1}$$

$$t_i = \frac{\left|\overrightarrow{S_iG}\right| + \left|\overrightarrow{GR_i}\right|}{C_P} \tag{2}$$

where m and n specify that the grid is on the m-th row and n-th column, N is the total number of measurements and C_P is the propagating velocity of longitudinal wave. The image intensity array can then be transformed into an image by color mapping. With this process, it extracts the information not just from one received signal but from all of them. In resultant image, the intensity will be summed up evidently when an interface exists right at the grid point and it will appear as a bright point. In contrast, it will be canceled out and represented as a dark point in the image. The intensity of the grids associated with defects or interfaces will be enhanced whereas that of the grids associated with uniform matrix will be reduced due to cross interference. With this image processing scheme, the defects and interfaces implied in the matrix material can be exposed. In this paper, high image intensity associated with defects and interfaces will be displayed with bright white while low intensity associated with uniform matrix will be displayed with dark black.

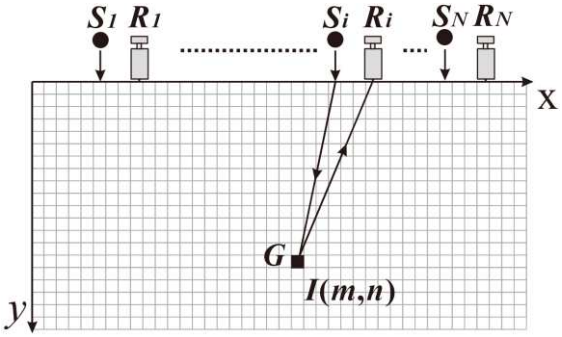

Figure 1 Schematic of operations and meshing of specimen for SAFT process.

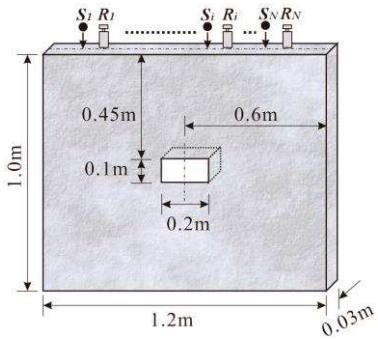

Figure 2 Dimensions of concrete slab with a rectangular void.

Consider a concrete slab with a rectangular void inside as shown in Figure 2. A plan-stress finite difference program was used for numerical simulation of wave propagation. Figure 3 shows the B-scan diagram of 25 received displacement signals in direction normal to recording surface. The fluctuation marked with "R", "B", "D" and "RR" represents the arrival wave of Rayleigh wave, the reflected longitudinal wave from bottom boundary, the reflected longitudinal wave from defect and Rayleigh wave reflected from side boundary. Shown in Figure 4 is the resultant SAFT image calculated with these 25 received signals, it is obvious there is a bright strip in the center indicating a discontinuous interface which is the upper surface of the void. It is not only the location but also the defect width could be defined on this image. To prevent the dynamic range of resultant image from being increased by first-arrived Rayleigh wave, 20 cm thick portion below the free surface was erased to a dark area to enhance the image contrast, Tong et al.

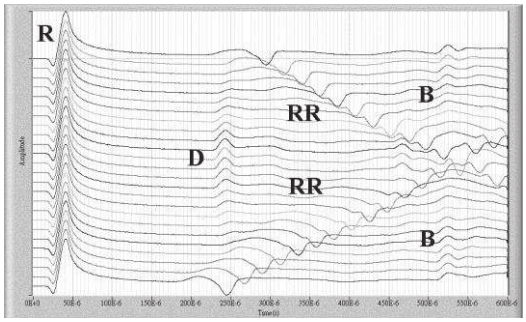

Figure 3 B-scan diagram of concrete slab with a rectangular void generated from simulated data.

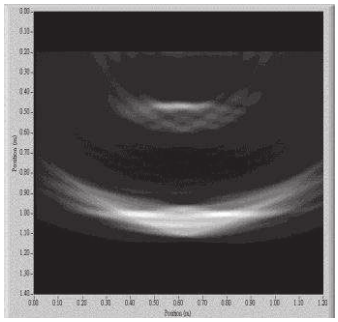

Figure 4 SAFT image of concrete slab with a rectangular void generated from simulated data.

3. COMPOSITION OF SYSTEM

The proposed imaging system is mainly composed of an impact source generator, a transducer, a signal capturing unit and a laptop with operation software, as shown in Figure 5. In the beginning of operation, the impact source generator generates an impact source by impacting a steel ball on the surface of specimen. A transducer receives surface response on the specimen's upper surface and then converts into electrical signal. A signal capturing unit amplifies the small signal and converts the analog signal into digital data for further process. Operation software controls all the measurement procedure and finally develops a resultant image. More detailed information about design and function of each component is described as follows.

3.1 Impact source generator

The impact source generator is made of a steel bar with a steel ball weld on the end. To generate elastic wave, the steel bar is bent and then released to hit specimen's surface. The force-time function of impact is almost in the form of half cycle $sin^{3/2}(t)$ function, Proctor et al. Derived from Hertz contact theory, Goldsmith et al, the contact time T_C could be expressed as:

$$T_C = 8.034\left[\frac{\rho_1(\delta_1+\delta_2)}{v_0^{1/2}}\right]^{2/5} R \tag{3}$$

While

$$\delta_1 = \frac{1-\nu_1^2}{\pi E_1} \qquad \delta_2 = \frac{1-\nu_2^2}{\pi E_2} \tag{4}$$

Where ν is Poisson's ratio, E is Young's modulus, v_0 is the impact velocity. The subscript 1 and 2 represent the character of steel ball and that of half-space respectively. R represents the radius of steel ball. From Eq.3 and Eq.4, it shows that contact time T_C is mainly dominated by the size of steel ball and is proportional to radius R.

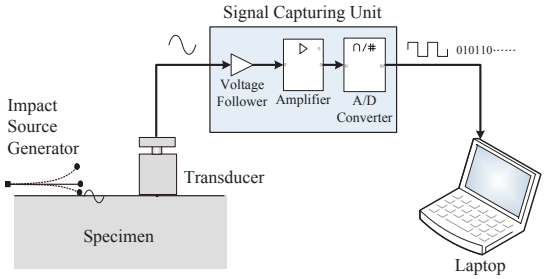

Figure 5 Composition of imaging system.

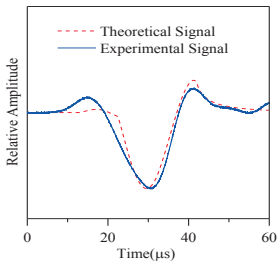

Figure 6 Signals of a 4mm steel ball impact.

Shown in Figure 6 are the theoretical and experimental time-domain displacement signals of a 4mm diameter steel ball shooting onto a concrete specimen which are received 5cm away from impact point. The theoretical signal is obtained from the analytical solution of transient normal load on a half-space, Achenbach et al. The force-time function was in the form of half cycle $\sin^{3/2}(t\pi/T_C)$ function which the contact time T_C was calculated from Eq.3 and Eq.4, where E_1= 205.3GPa，E_2= 33.6GPa，ν_1=0.293，ν_2=0.188，v_0= 1.764m/s. The experimental signal was obtained by free-falling a 4mm steel ball from a height of 0.3m onto the surface of a concrete specimen. It can be found a very high similarity between the two time-domain waveforms from Figure 6. Shown in Figure 7 are the spectrums of these two signals. The central frequency of elastic wave calculated from the analytical solution is very close to that from the experimental signal which was measured on a real concrete specimen. It means the period of dominating elastic wave can be estimated from Eq. 3 and Eq. 4 while the size of steel ball is selected. Therefore it can be guidance for choosing a proper size steel ball as the impact source when making the trade-off between resolution and detectable depth which is often an opposite issue for in-situ NDT applications.

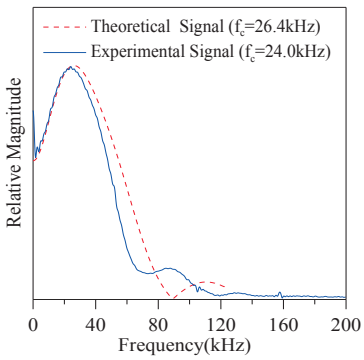

Figure 7 Spectrums of time-domain signals.

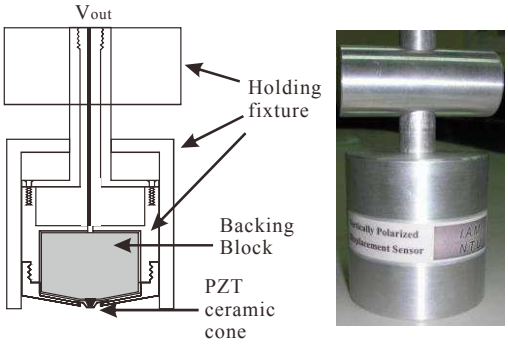

Figure 8 Design and end item of displacement transducer.

3.2 Transducer

To convert mechanical displacement signal into electrical signal, a transducer is designed for this imaging system. It is mainly composed of a PZT ceramic cone, a backing block and the holding fixture as shown in Figure 8. The axially polarized PZT ceramic cone generates an electric potential difference between two electrodes when suffered axial deformation so that the

output voltage is proportional to the displacement amplitude received by the transducer. The upper electrode is electrically connected to the backing brass block and then to the BNC connector as the signal output. The lower electrode is electrical ground which is electrically connected to a copper film, through the holding fixture and finally reaching the BNC connector.

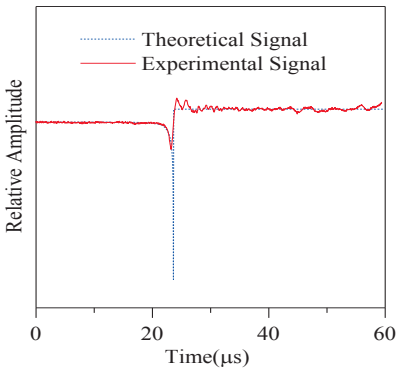

Figure 9 Theoretical and experimental signals of glass capillary cutting experiment.

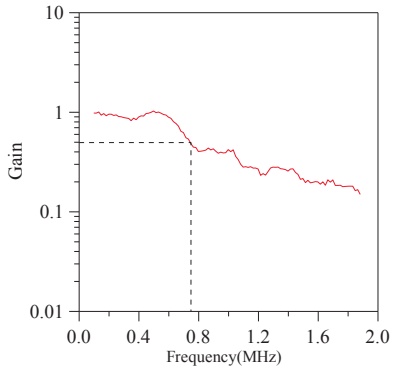

Figure 10 Frequency response of the designed transducer.

To verify the adaptability of the transducer for the imaging system, a calibration experiment on a steel block was conducted. The wave source was generated by cutting a glass capillary on the specimen surface to simulate a normal concentrated load with the form of Heaviside function, Breckenridge et al, Kim et al. Shown in Figure 9 are the displacement signals, without boundary reflection, received 7cm away from wave source. The dotted line represents the theoretical signal, while the solid line represents the experimental signal received by the transducer described above. These two signals are quite consistent except the high frequency components owing to the limitation from the frequency response of the transducer. Shown in Figure 10 is the frequency response of the transducer calculated by frequency domain decovolution from previous two signals. The result shows the transducer can handle signals whose frequency is about lower than 700 kHz. It is high enough for the proposed imaging system whose center frequency of elastic wave is typically lower than 10 kHz.

3.3 Signal capturing unit

The signal capturing unit consists of a voltage follower, an amplifying circuit, and an A/D converter. The voltage follower is a good signal buffer with very high input impedance so that signal from transducer with very small current will not be distorted. Then the received signal is enhanced by an adjustable amplifying circuit which is mainly composed of a differential voltage amplifier with high capability of rejecting environmental random noise. The amplified analog signal is digitized by an A/D converter for further process. The sampling rate of a 16-bit A/D converter is 20MSPS(Mega Samples per Second) which is high enough for elastic wave signal capturing in proposed system whose center frequency of received signal is around 1k Hz to 100k Hz typically.

3.4 Operation software

In proposed imaging system, the operation software is used not only for data processing but also controlling the signal capturing unit. By operating the control panel shown in Figure 11, the measurement parameters could be set up and resultant image will be generated right after several impact-and-receive measurements. There is one important thing need to note that the elastic wave source in experiment is different from that in theoretical analysis. For ideal

situation amplitude of elastic wave source in each impact-and-receive measurement can be the same, while it varies in real world because the mechanical impact is hardly repeatable. Fortunately, amplitude of fist-arrived Rayleigh wave is proportional to impact force if the distance between source and receiver keeps unchanged. In the operation software, it normalizes received signals according to the amplitude of fist-arrived Rayleigh wave in each signal to keep equal weighting of received signals to form a B-scan diagram. After that, a 2D-array representing the image intensity will be formed according to Eq.(1) with all equal-weighted signals. Finally the resultant image will be generated by mapping image intensity into brightness of each image pixel.

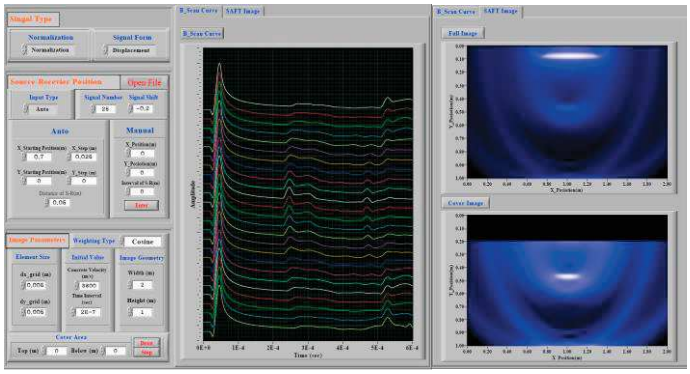

Figure 11 Control panel of proposed imaging system.

4. EXPERIMENTAL RESULTS

To confirm the usability of the proposed imaging system, a 3cm thick defective concrete slab was cased for experiment whose detailed dimension is shown in Figure 2. To build an artificial void, a styrofoam bar with a wood cover was instead fixed at the design position while the concrete slab was cast. After curing, the styrofoam bar and its wood cover were removed. The experiment was carried out with a series of impact-and-receive operations on the top surface of concrete slab. The elastic wave was generated by impacting the specimen's surface with an 8 mm steel ball and the surface response was then received by the above-mentioned transducer. Distance between impact source and receiver kept to be 5cm. Operation interval from current impacting point to the next one is 5cm. The first operation was performed at the point which is 30cm from the edge of concrete slab. In this experiment, 14 displacement responses were recorded for image construction.

Shown in Figure 12 is the B-scan diagram composed of 14 displacement responses received on specimen's surface. On this diagram dotted line marked with D, R and RR represents reflected longitudinal waves from upper surface of rectangular void, direct-arrived Rayleigh waves and reflected Rayleigh waves from side boundary respectively. It appears as though void embedded inside concrete specimen could be defined on this conventional B-diagram but not quite straightforward. Shown in Figure 13 is the SAFT image generated by proposed imaging system. In the center of image, it is easy to define a bright zone as the profile of artificial void's upper surface. As compared to conventional B-scan diagram, SAFT image can provide better results to identify defect's location, size, and even front-end shape more straightforwardly. The experimental result shows good agreement with numerical simulation shown in Figure 4. It also exhibits the potential of proposed imaging system to reveal defects embedded inside in-situ concrete structures by imaging.

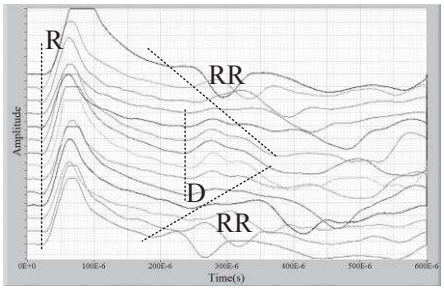

Figure 12 Experimental B-scan diagram of defective concrete slab.

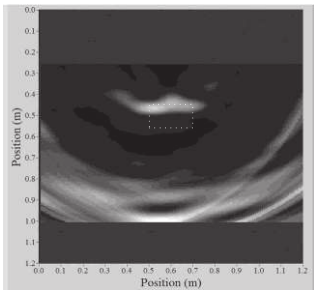

Figure 13 Experimental SAFT image of defective concrete slab.

5. CONCLUSIONS

In general defect inspection tasks for concrete structures, the testing environment is often dangerous and inconvenient for the operator. It is very important to provide a handy tool for in-situ inspection. The state-of-the-art technologies could provide enough assistance to the development of instrument on reducing the size and simplifying the operation procedure. In this paper, it integrates the advantages of point-source/point-receiver scheme and SAFT process to develop a portable defect imaging system for revealing defects inside concrete structures. The impact source generator can generate high-energy elastic wave with its mechanical mechanism so elastic wave can propagate deeper and carry more information back. Result of steel ball free-falling experiment shows that the center frequency of generated wave can be estimated by the method proposed in this paper. In other words, the wavelength of dominating wave can be changed by selecting a corresponding steel ball as the impactor. For surface response capturing, a transducer was designed and calibrated. Result of glass capillary cutting experiment shows this transducer can handle the signal of transient elastic wave whose frequency composition is below 700 kHz so it is adequate to be a receiver in the proposed imaging system. With the help of operation software, the imaging system can generate an image immediately after a series of impact-and-receive operations. It means that the operator can examine the integrity of inspected specimen instead of post-analyzing in laboratory. In the concrete slab experiment, the result obtained with this system shows good agreement with that simulated by finite difference method not only on B-scan diagram but also on SAFT image. The resultant image reveals the information about location, size, and front-end shape of the artificial void. It demonstrates great potential of proposed imaging system on detecting defects of in-situ concrete structures.

6. ACKNOWLEDGMENT

The authors thank the National Science Council of ROC for the financial support of this research through the grant NSC 94-2211-E-241-017.

7. REFERENCES

Achenbach, JD, Wave propagation in elastic solids, North-Holland, New York, 1973.

Breckenridge, FR, Tschiegg, CE, Greenspan, M, Acoustic emission: some applications of Lamb's problem, J. Acoust. Soc. Am, 57(1975), 3, 626-631.

Carino, NJ, Sansalone, M, Detection of voids in grouted ducts using the impact-echo method, ACI Mater. J., 89(1992), 3, 296-303.

Goldsmith, W, Impact: The theory and physical behavior of colliding solids, Edward Arnold Ltd., London, 1960.

Jerzy, Hola, Krzysztof, Schabowicz, State-of-the-art non-destructive methods for diagnostic testing of building structures - anticipated development trends. Archives of Civil and Mechanical Engineering. (2010), 10, 3, p. 5-18.

Jerzy, Hola, Lukasz, Sadowski, Krzysztof, Schabowicz, Nondestructive identification of delaminations in concrete floor toppings with acoustic methods. Automation in Construction. (2011), 20, 7, p. 799-807.

Kim, YH, Kim, HC, Source function determination of glass capillary breaks, J. Phys. D: Appl. Phys. 26(1993), 253-258.

Liu, PL, Lee, KH, Wu, TT, Kuo, MK, Scan of surface-opening cracks in reinforced concrete using transient elastic waves, NDT & E Int., 34(2001), 219-226.

Malhotra,VM, Carino, NJ, CRC handbook on nondestructive testing of concrete, CRC Press, Inc, 1991, 169-188.

Proctor, TM, Breckenringe, FR, Source force waveforms: the use of a calibrated transducer in obtaining an accurate waveform of a source, J. Acoust. Emiss, 10(1991), 3, 43-48.

Tong, JH, Liao, ST, Lin, CC, A new elastic-wave-based imaging method for scanning the defects inside the structure, IEEE Trans. Ultrason. Ferroelectr. Freq. Control, 54(2007), 1, 128-137.

Tong, JH, Chiu, CL, Wang, CY, Improved Synthetic Aperture Focusing Technique by Hilbert-Huang Transform for Imaging Defects inside a Concrete Structure, IEEE Trans. Ultrason. Ferroelectr. Freq. Control, 57(2010), 11, 2512-2521.

Wu, TT, Fang, JS, A new method for measuring concrete elastic constants using horizontally polarized conical transducers, J. Acoust. Soc. Am, 101(1997), 1, 330-336.

Wu, TT, Fang, JS, Liu, GY, Kuo, MK, Detection of elastic constants of a concrete specimen using transient elastic waves, J. Acoust. Soc. Am, 98(1995), 4, 2142-2148.

Wu, TT, Fang, JS, Liu, PL, Detection of the depth of a surface-breaking crack using transient elastic waves, J. Acoust. Soc. Am, 97(1995), 1678-1686.